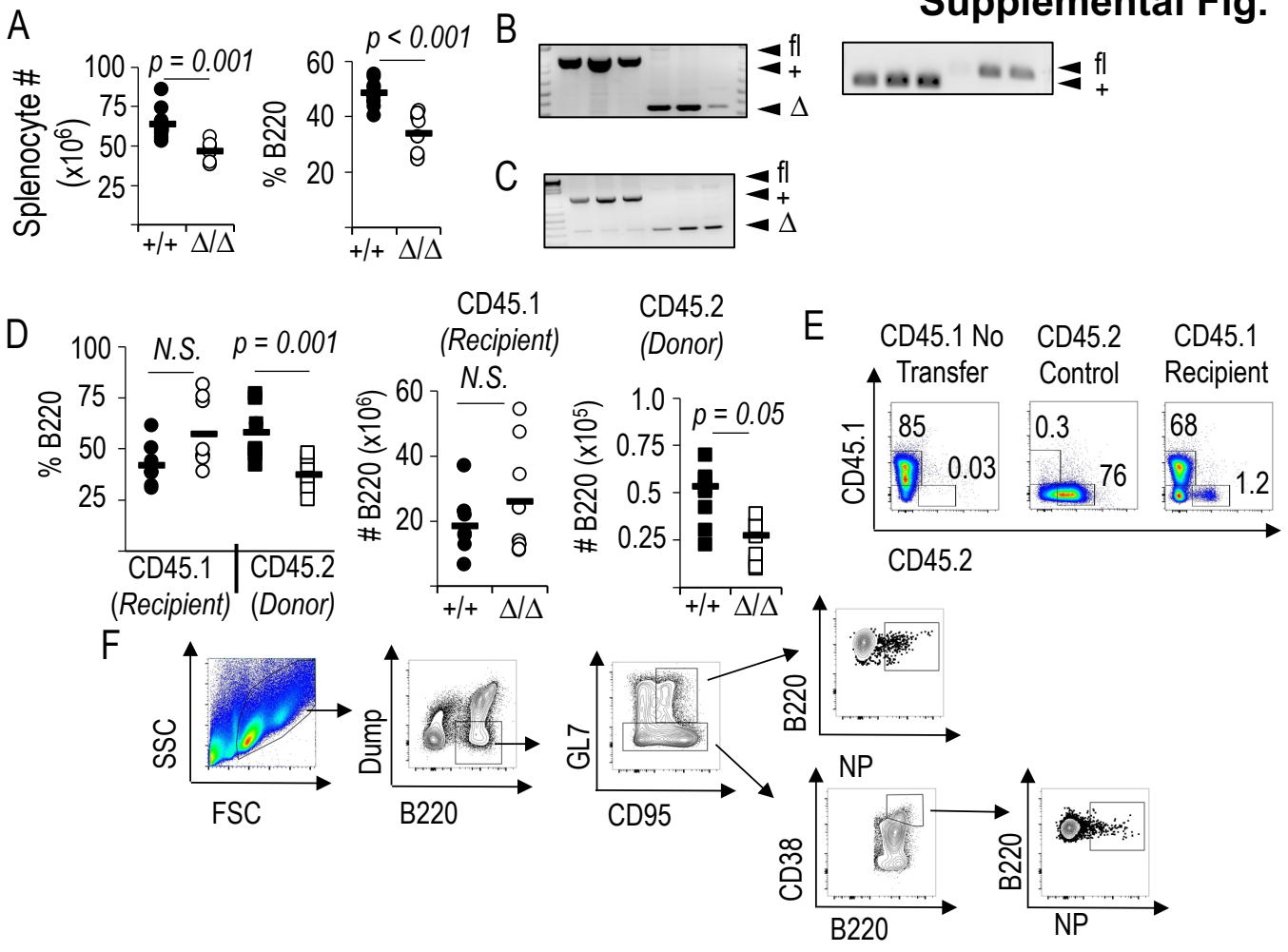

Supplemental Figure 1. B cell population sizes after prolonged loss of Raptor. (A) B cells from tamoxifen-injected huCD20-CreER^{T2+} *Rptor*$^{+/+}$ (filled symbols) and *Rptor*$^{f/f}$ huCD20-CreER^{T2+} mice (as in Fig. 2A) were quantified at the point of harvest by flow cytometry. Raw data for cellular recoveries in spleens of huCD20-CreER ^{T2} mice at harvest after serial tamoxifen injections followed by immunization and boosting as described in the Methods and illustrated in Fig. 2A. Left panel, total counts of Trypan Blue-excluding spleen cells; right panel, fraction of each spleen that was B220^{+}. (B, C) Tamoxifen-driven Cre excision of the flox segment of the *Rptor* gene. (B) Shown are the allele-specific products of *Rptor* PCR with DNA from pools of donor B cells [WT (*Rptor*$^{+/+}$ *Rosa26*-CreER^{T2+}) and Raptor-deficient (*Rptor*$^{Δ/Δ}$ *Rosa26*-CreER^{T2+}) prior to transfer into allotype-disparate recipient mice (IgH^{a} or CD45.1). (C) Maintenance of the *Rptor*-deleted allele after immunization experiments with huCD20-CreER^{T2}. (D) Graphical representation of % (left) and number (right panels) of donor and recipient B cells after immunization in transfer experiments. Each point represents one of the six mice of each genotype, equally distributed across three biologically independent replicate experiments. Shown are the percent (left graph) and numbers (right two graphs) of recipient (circles) vs donor (squares) B cells [WT, filled symbols, and Raptor-deficient (*Rptor* $^{Δ/Δ}$), open symbols] harvested after transfers into B6-CD45.1 recipients and immunization (as in Fig. 1A). Each point represents one of 8 mice of each genotype distributed across three biologically independent replicate experiments. (E) Representative example of background signal in the immune fluorescent analyses distinguishing donor (CD45.2) from recipient (CD45.1) hematopoietic cells. Shown are (leftmost panel) the combined anti-CD45.1 and anti-CD45.2 signals obtained with a B6-CD45.1 control (no donor cells), the same staining applied to a B6-CD45.2 control (no donor cells) (middle panel), and (rightmost panel) a representative sample from the same experiment, to illustrate a donor-derived population in its recipient setting. (F) Representative gating strategy for analyzing B cells harvested from mice or cultures, here showing gates leading to displays of Ag-specific germinal center and memory B cells.

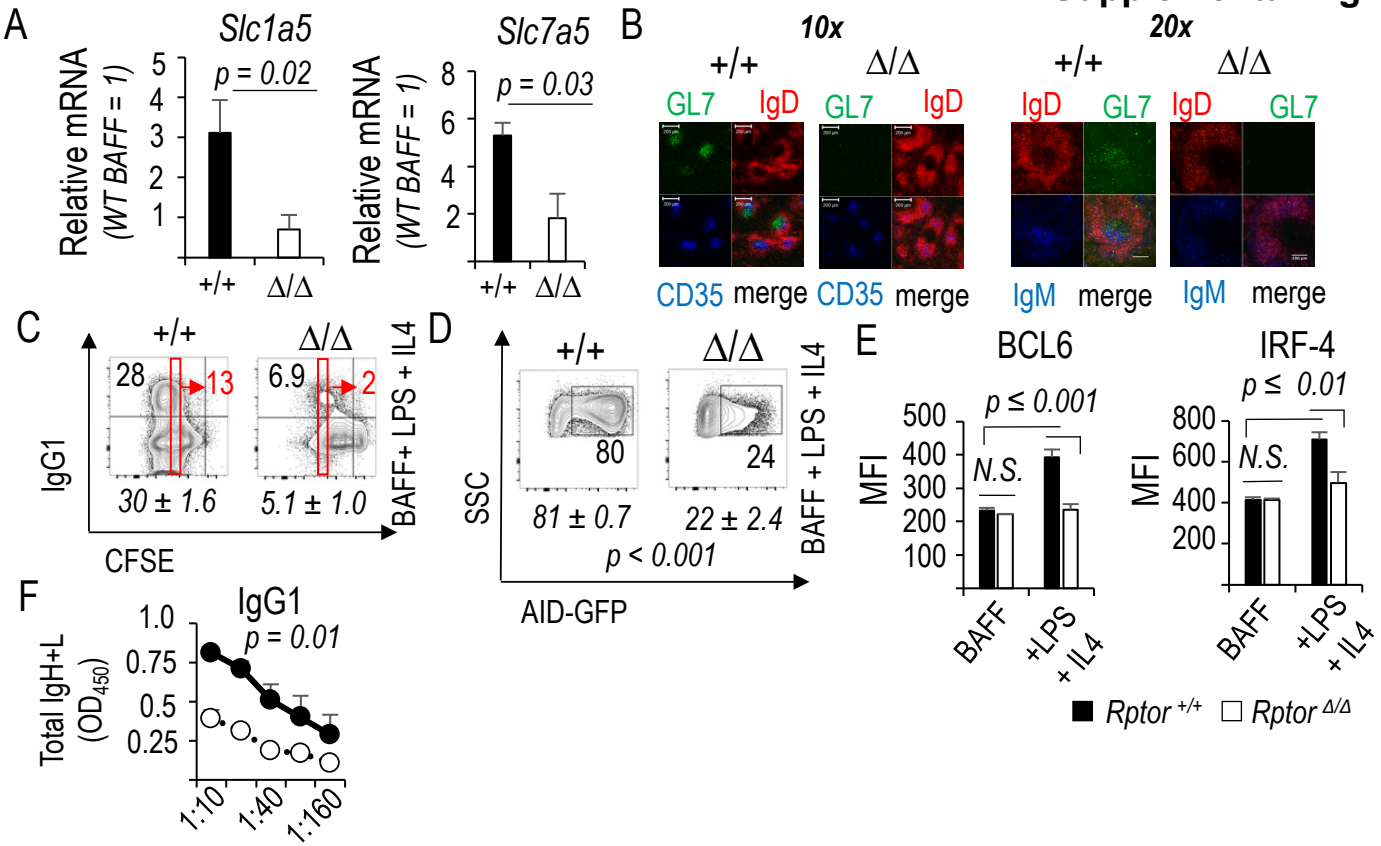

Supplemental Figure 2. Metabolic reprogramming and reduced class-switching after mTORC1 inactivation. (A) Reduced transporters for mTORC1-inducing amino acids. WT (Raptor$^{+/+}$ *Rosa26*-CreER^{T2+}) and Raptor-deficient (Raptor$^{\Delta/\Delta}$ *Rosa26*-CreER^{T2+}) B cells were cultured (2 d) with BAFF, or BAFF, LPS and IL-4, then harvested into Trizol reagent. mRNAs encoding *Slc1a5* and *Slc1a7* were analyzed by qRT^2-PCR, normalizing each analysis to the value for WT BAFF only (little to no difference was observed in baseline expression). (B) Germinal center architecture is promoted by mTORC1 in B cells. Shown are representative immunofluorescence microscopy images generated with spleens from tamoxifen-injected huCD20-CreER$^+$ *Rptor* $^{+/+}$ and huCD20-CreER$^+$ *Rptor* $^{\Delta/\Delta}$ mice 7 d after immunization with SRBC as described (11) (10x left, 20x right). (C) mTORC1 regulates antibody class switch. WT (*Rptor*$^{+/+}$ *Rosa26*-CreER^{T2+}) and Raptor-deficient (*Rptor* $^{\Delta/\Delta}$ *Rosa26*-CreER^{T2+}) B cells were loaded with CFSE, activated with LPS and cultured for four days in the presence of BAFF and IL-4. Shown are flow cytometry measurements of division history (CFSE fluorescence) versus surface IgG1-expression on B cells from one experiment representative of three independent experiments with a total 5 mice of each genotype distributed across the independent replicates. A measurement gate at the same fluorescence intensity band (same multiple divisions) is included to highlight the reduced frequency of IgG1$^+$ cells (numbers from this restricted gate to the right of the rectangle) as a variable independent from division efficiency. (D) AID-GFP fluorescence was quantified by flow cytometry after AID-GFP$^+$ WT (*Rosa26*-CreER^{T2+} *Rptor*$^{+/+}$) and Raptor-deficient (*Rosa26*-CreER^{T2+} *Rptor* $^{\Delta/\Delta}$) B cells were purified and cultured as in (C). Shown are flow plots of one sample pair representative of 4 independent replicate experiments, with inset numbers showing the frequency of GFP$^+$ cells in the individual analysis and *mean* (± SEM) values italicized. (E) mTORC1 required for activation-induced increases of BCL6 and IRF4 in B cells in vitro. WT (*Rptor*$^{+/+}$ *Rosa26*-CreER^{T2+}) and Raptor-deficient (*Rptor* $^{\Delta/\Delta}$ *Rosa26*-CreER^{T2+}) B cells were cultured in BAFF alone (to maintain quiescent survival) or activated with LPS and cultured (2 d) in BAFF and IL-4. Cells were then analyzed by flow cytometry after staining for intracellular BCL6 or IRF4, as indicated and as in Fig. 3C. Shown are the mean (±SEM) values for mean fluorescent intensity of the transcription factor stains in the gate for viable B cells, derived from four samples of each genotype equally distributed in two separate replicate experiments. (F) Mean (±SEM) ELISA results measuring IgG1 in culture supernatants from WT (*Rptor*$^{+/+}$ *Rosa26*-CreER^{T2+}) and Raptor-deficient (*Rptor* $^{\Delta/\Delta}$ *Rosa26*-CreER^{T2+}) B cells cultured as in (C). The mean titration curve of values measured in four biologically independent experiments is shown. Statistical significance between WT and KO samples was analyzed by pair-wise testing at the 1:10, 1:20, and 1:40 dilutions of culture supernatants.

Supplemental Fig. 3

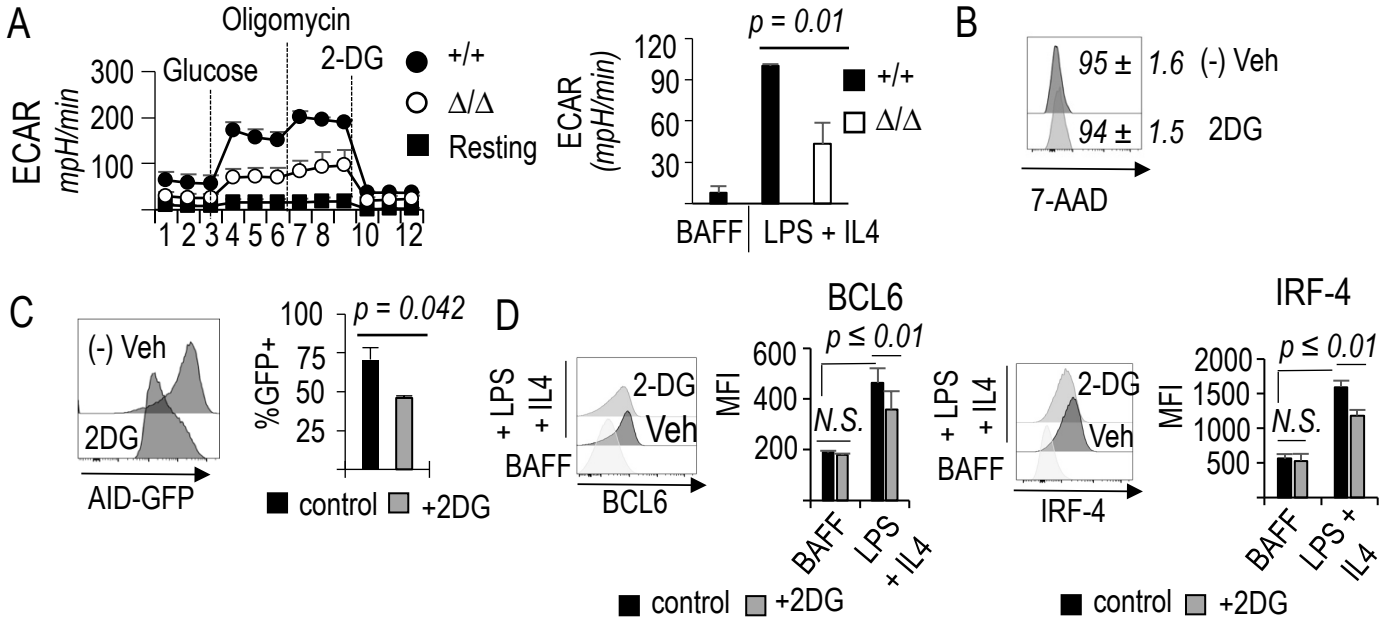

Supplemental Fig. 3. Glycolysis rate modulates BCL6, IRF-4, and AID. (A) mTORC1 promotes activation-dependent glycolytic metabolism in B cells. WT (*Rptor*$^{+/+}$ *Rosa26*-CreER^{T2+}) and Raptor deficient (*Rptor*$^{f/f}$ *Rosa26*-CreER^{T2+}) B cells were cultured for 2 days with BAFF (resting), or BAFF, LPS and IL4. Cells were then counted and equal numbers of viable cells were plated on Seahorse assay plates to measure glycolysis with a Seahorse XFe metabolic flux analyzer. (Left portion) Mean (±SEM) glycolytic profiles of 5 independent replicate experiments are shown, with each error bar representing the standard error of the mean pooling data at the same point of the analyzer program in the five experiments. (Right portion) Shown are mean (±SEM) basal extracellular acidification rates of WT and Raptor-deficient B cells prior to addition of glucose, with data from the five independent replicate experiments. (B, C) Glycolytic flux regulates inducibility of AID expression. WT B cells were cultured for 4 days in complete RPMI media with BAFF, LPS, and IL-4 in the presence or absence of 2-deoxyglucose (2-DG), which did not alter B cell viability as compared to control cultures (B). (C) GFP fluorescence in the viable lymphoid population gate (FSC x SSC, 7-AAD^{neg}, B220^{+}) was measured for AID-GFP^{+} B cells cultured as in (A) but in the presence or absence of 2DG. A representative histogram of AID-GFP in control and 2-DG treated cells is shown. Right panel: Quantification of the mean (±SEM) percent GFP positive (AID^{+}) cells in four independent replicate experiments. (D) Reduced glycolysis impairs induction of BCL6 and IRF4 expression. WT B cells were activated and cultured as in panel A but in the presence or absence of 2DG, followed by intracellular staining of BCL6 and IRF4 and flow cytometry. Bar graphs display mean (±SEM) MFI values for each sample under the indicated conditions in three biologically independent replicate experiments.

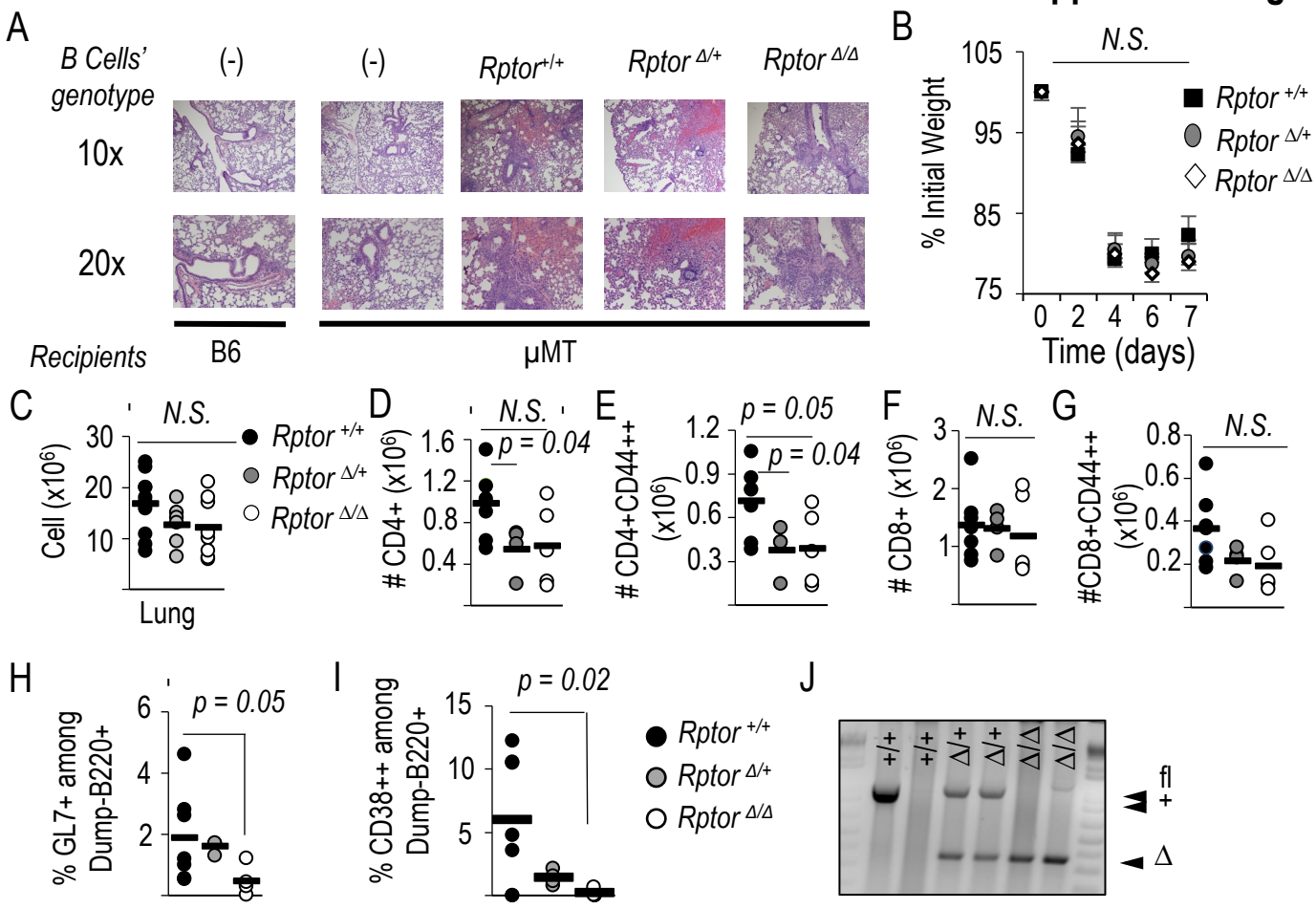

Supplemental Fig. 4. Minimal protection against heterologous influenza challenge. (A) Representative hematoxylin & eosin-stained lung sections after harvest from the influenza X- 31-inoculated mice of indicated types from the experiments of Fig. 1, documenting inflammation in the recipients of *Rptor* $^{+/\Delta}$ and *Rptor* $^{\Delta/\Delta}$ B cells as compared to the infected recipients of WT B cells. (B, C) Mean (±SEM) weight changes (B), and (C) cellularity of lung infiltrates of the same mice as in (A), after i.n. inoculation with the X-31 challenge strain. In panel B, pair-wise testing of the null hypothesis for a difference between recipients of WT versus mutant B cells at each time point indicated a lack of statistical significance (symbolized by N.S. across the full time course). Weight data measured for each mouse are plotted after normalizing to the weight prior to infection. In panel C, similar pair-wise comparisons of WT to mutant samples fell short of statistical significance ("N.S.") for each comparison. Subsets of lung-infiltrating T cells determined from the recovered cell numbers (C) and flow phenotyping of (D) total or (E) activated CD44^{hi} CD4^{+} T cells, and (F) total or (G) activated CD44^{hi} CD8^{+} T cells after enzymatic dispersion of recovered lung tissue of the indicated recipient mice. "N.S." in panels F and G are as for panel C. (H, I) Percentages of flow-phenotyped GC B cells (dump^{neg} B220^{+} GL7^{+}) (H) and (I) memory B cells (dump^{neg} B220^{+} GL7^{neg} CD38^{++}) in spleens of the X-31-challenged mice.